Steel and Composite Structures, *Vol. 36, No. 1* (*2020*) *63-74*
DOI: https://doi.org/10.12989/scs.2020.36.1.063

Post-buckling analysis of geometrically imperfect tapered curved micro-panels made of graphene oxide powder reinforced composite

Seyed Sajad Mirjavadi[1], Masoud Forsat*[1], Mohammad Reza Barati[2] and AMS Hamouda[1]

[1]*Department of Mechanical and Industrial Engineering, Qatar University, P.O. Box 2713, Doha, Qatar*
[2]*Fidar project Qaem Company, Darvazeh Dolat, Tehran, Iran*

(*Received March 25, 2020, Revised June 6, 2020, Accepted June 9, 2020*)

Abstract. The present research investigates post-buckling behavior of geometrically imperfect tapered curved micro-panels made of graphene oxide powder (GOP) reinforced composite. Micro-scale effects on the panel structure have been included based on strain gradient elasticity. Micro-panel is considered to be tapered based on thickness variation along longitudinal direction. Weight fractions of uniformly and linearly distributed GOPs are included in material properties based on Halpin-Tsai homogenization scheme considering. Post-buckling curves have been determined based on both perfect and imperfect micro-panel assumptions. It is found that post-buckling curves are varying with the changes of GOPs weight fraction, geometric imperfection, GOP distribution type, variable thickness parameters, panel curvature radius and strain gradient.

Keywords: Post-buckling; cylindrical shell; strain gradient theory; nano-composite material; curved panel

1. Introduction

In the field of materials science, there are various types of composite materials such as fiber reinforced composites, functionally graded (FG) material, nano-particle reinforced composites and etc (Abdelaziz *et al.* 2017, Addou *et al.* 2019, Mirjavadi *et al.* 2017, 2018, 2019, Azimi *et al.* 2017). Each of the may represent specific properties is desirable directions (Boukhlif *et al.* 2019, Thanh *et al.* 2019, Zarga *et al.* 2019, Ahmed *et al.* 2019). Reinforcement of matrix materials is a key idea for enhancing their mechanical properties and this task can be done using different types of fibers or even nano-scale inclusions (Vo *et al.* 2017, Houari *et al.* 2018). Recently, nano-scale inclusions are shown to provide excellent interaction with the matrix material (Marami *et al.* 2016) leading to a novel type of material called nano-composite material.

Due to remarkable stiffness and mechanical character of carbon nanotube and graphene, they are broadly employed as reinforcement particles (Wu *et al.* 2017, Zhao *et al.* 2017, Bakhadda *et al.* 2018). Graphene oxide powders are another type of nano inclusions which can be derived from graphite mass oxidation. Based on recent studies, it is proved that graphene oxide powders are compatible with different matrix materials such as polymeric and metallic materials. Graphene oxide composites demonstrate remarkable Young modulus and tensile strength as are carbon-based material with remarkable performances and low costs. Due to aforementioned reasons, many authors devoted their efforts to examine mechanical properties of graphene reinforced structures. An investigation on post-buckling properties of nano-composite beams reinforced by graphene sheets has been performed by Barati and Zenkour (2017). Ebrahimi and Dabbagh (2019) examined free vibrations of plates reinforced by combined fibers and nanotubes. Also, Ebrahimi *et al.* (2019) researched thermal effects on dynamic properties of a graphene oxide powder reinforced plate. Most recently, Zhang *et al.* (2020) explored bending and buckling of graphene oxide reinforced beams. Based on provided information, it can be concluded that post-buckling analysis of graphene-oxide reinforced curved panels with variable thickness and geometric imperfections has not performed yet.

In some cases including space structures and micro-mechanical engineering for which the decrement in weight is of great importance, the panels with variable thickness are the best option. The employment of variable thickness could aid the engineers and researches diminish the weight of curved structure leading to shape optimization processes which allows to distribute and enhance the stiffness in the utmost stressed regions of the structure. Such structures having variable thickness, indeed, could represent better actions in deflection, buckling and vibrations when compared to a structure having un-varied thickness. This issue is studied by some researchers (Thang *et al.* 2016, Nguyen *et al.* 2020).

Recent studies on micro-scale structures proved that the strain field at such scales may be not uniform and it must be considered as non-uniform due to strains gradients (Barati 2018). Classic elasticity is not able to incorporate such non-uniform strain fields since it is not designed for micro-scales. By adding scale factors, strain gradient elasticity can include the effects of the strain gradient components. This theory is widely applied in mechanical analysis of micro-size structures with different types of materials (Li *et al.* 2017, Barretta *et al.* 2018, She *et al.* 2019). These studies reported additional stiffness of the micro-scale structure

*Corresponding author, Professor
E-mail: masoudforsatlar@gmail.com

ISSN: 1229-9367 (Print), 1598-6233 (Online)

compared to a macro-scale counterpart.

Considering geometric imperfection effects, this article studies post-buckling behavior of geometrically imperfect tapered curved micro-panels constructed from GOP-reinforced composite. Classic shell theory has been utilized for modeling of the panel. The classical plate and shell models can be appropriately deduced form the classical elasticity formulation of the Saint-Venant flexure problem (Faghidian 2016). However, shear deformation effect is neglected in the classic shell theory (Ali Faghidian 2017). In order to incorporate small scale influences, strain gradient theory has been utilized. The thickness of micro-scale panel is assumed to be variable in longitudinal direction. Employing Halpin-Tsai micro-mechanical model, the material properties of nanocomposite material based on uniformly and linearly distributed GOPs have been obtained. Post-buckling curves have been determined based on both perfect and imperfect micro-panel geometries. It will be illustrated that post-buckling curves are affected by the values of GOP amount, strain gradient coefficient, variable thickness parameters, panel radius, geometric imperfection and also GOP distribution type.

2. Elastic properties for GOP-reinforced composites

Based on Halpin-Tsai micro-mechanic model, it is assumed that the Young modulus of the nano-composite ($\tilde{E}$) is a function of GOPs volume (V_{GOP}) and Young modulus of matrix phase (E_M) as (Zhang *et al.* 2020)

$$\tilde{E}=0.49\left(\frac{1+\xi_L^{GOP}\eta_L^{GOP}V_{GOP}}{1-\eta_L^{GOP}V_{GOP}}\right)E_M +0.51\left(\frac{1+\xi_W^{GOP}\eta_W^{GOP}V_{GOP}}{1-\eta_W^{GOP}V_{GOP}}\right)E_M \tag{1}$$

so that ξ_L^{GOP} and ξ_W^{GOP} define two geometrical factors indicating the impacts of graphene configuration and scales as

$$\xi_L^{GOP}=\frac{2d_{GOP}}{t_{GOP}} \tag{2a}$$

$$\eta_L^{GOP}=\frac{\left(E_{GOP}/E_M\right)-1}{\left(E_{GOP}/E_M\right)+\xi_L^{GOP}} \tag{2b}$$

$$\xi_W^{GOP}=\frac{2d_{GOP}}{t_{GOP}} \tag{2c}$$

$$\eta_W^{GOP}=\frac{\left(E_{GOP}/E_M\right)-1}{\left(E_{GOP}/E_M\right)+\xi_W^{GOP}} \tag{2d}$$

so that d_{GPL} and t_{GPL} define GOP average diameter and thickness, respectively. In this study, two kinds of GOP distributions have been selected which are uniform and linearly graded. Accordingly, the volume of GOP based on the two kinds of distribution can be introduced as

$$\text{Uniform:}\quad V_{GOP}=V_{GOP}^{*} \tag{3}$$

$$\text{Linear:}\quad V_{GOP}=(1+2\frac{z}{h})V_{GOP}^{*} \tag{4}$$

in which V_{GOP}^{*} is a function of GOP weight fraction (W_{GOP}) as well as densities of GOP and matrix (ρ_{GOP} , ρ_M) and can be calculated as

$$V_{GOP}^{*}=\frac{W_{GOP}}{W_{GOP}+\frac{\rho_{GOP}}{\rho_M}-\frac{\rho_{GOP}}{\rho_M}W_{GOP}} \tag{5}$$

Another important factor which can be determined based on rule of mixture is Poisson's ratio of GOP-reinforced composites ($\tilde{\nu}$) as a function of matrix volume ($V_M=1-V_{GOP}$) and Poisson's ratios of GOP and matrix (ν_{GOP} , ν_M) as

$$\tilde{\nu}=\nu_{GOP}V_{GOP}+\nu_M V_M \tag{6}$$

3. Mathematical modeling for tapered curved panel

Based on thickness variation from h_0 to h_1 in longitudinal direction, Fig. 1 illustrates a tapered curved micro-panel having curvature radius of R. For describing longitudinal variation of the panel thickness, the below definition of thickness has been used

$$h=h_0(1+g_1x^{g_2}) \tag{7}$$

in which g_2 denotes non-uniform parameter of varied thickness. Selecting $g_2=0$ the thickness has un-varied; g_2=1 defines the linear thickness variation and g_2=2 defines the parabolic thickness variation. Moreover, g_1 is a factor which evaluates the rate of changes in thickness

$$g_1=\frac{h_0-h_1}{h_0} \tag{8}$$

There are various plate/shell theories introduced in the literature (Abualnour *et al.* 2019, Balubaid *et al.* 2019, Batou *et al.* 2019, Belbachir *et al.* 2019, Bellal *et al.* 2020, Boulefrakh *et al.* 2019, Boutaleb *et al.* 2019, Semmah *et al.* 2019, Tlidji *et al.* 2019, Zaoui *et al.* 2019, Abdulrazzaq *et al.* 2020, Ahmed *et al.* 2019, Ahmed *et al.* 2020, Alasadi *et al.* 2019, Al-Maliki *et al.* 2019, Faleh *et al.* 2018, Faleh *et al.* 2020, Fenjan *et al.* 2019, Hamad *et al.* 2019, Khalaf *et al.* 2019, Kunbar *et al.* 2019, Muhammad *et al.* 2019, Fenjan *et al.* 2020, Al-Maliki *et al.* 2020).

The tapered curved micro-panel may be formulated employing thin shell model which represents the strain components as below forms

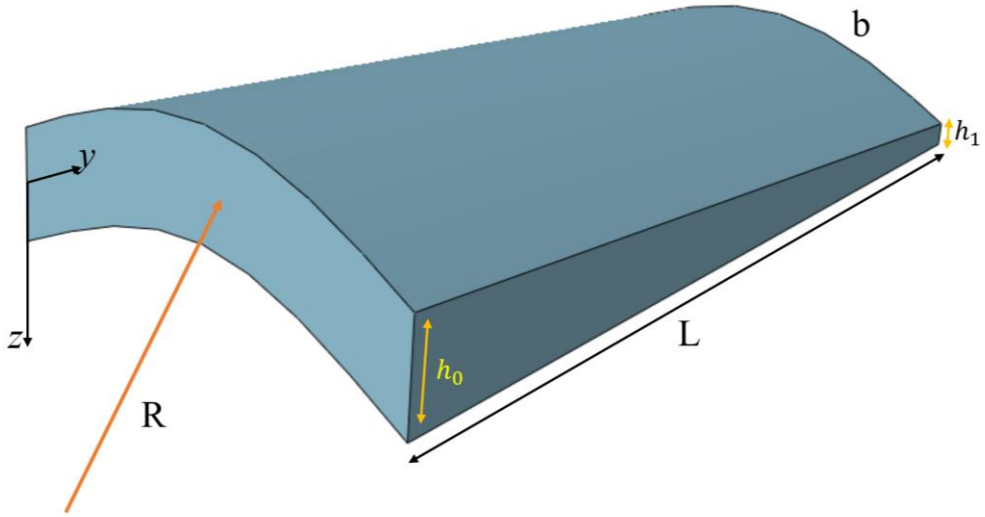

Fig. 1 Geometry of curved micro-panel with variable thickness

$$\begin{Bmatrix} e_x \\ e_y \\ \gamma_{xy} \end{Bmatrix} = \begin{Bmatrix} e_x^0 \\ e_y^0 \\ e_{xy}^0 \end{Bmatrix} - z \begin{Bmatrix} k_x \\ k_y \\ 2k_{xy} \end{Bmatrix} \tag{9}$$

in which

$$\begin{aligned} e_x^0 &= \frac{\partial u}{\partial x} + \frac{1}{2}(\frac{\partial w}{\partial x})^2 + \frac{\partial w}{\partial x}\frac{\partial w^*}{\partial x}, \\ e_y^0 &= \frac{\partial v}{\partial y} + \frac{1}{2}(\frac{\partial w}{\partial y})^2 + \frac{\partial w}{\partial y}\frac{\partial w^*}{\partial y} - \frac{w}{R}, \\ e_{xy}^0 &= \frac{\partial u}{\partial y} + \frac{\partial v}{\partial x} + \frac{\partial w}{\partial x}\frac{\partial w}{\partial y} \\ &+ \frac{\partial w}{\partial x}\frac{\partial w^*}{\partial y} + \frac{\partial w}{\partial y}\frac{\partial w^*}{\partial x}, \\ k_x &= \frac{\partial^2 w}{\partial x^2},\ k_y = \frac{\partial^2 w}{\partial y^2},\ k_{xy} = \frac{\partial^2 w}{\partial x \partial y} \end{aligned} \tag{10}$$

Defined strains incorporates deflection (w) and in-plane (u, v) displacements. Also, w^* defines the deflection due to imperfectness. In the case of micro-size structures, the relations for stresses σ_i (i=x, y, xy) may be defined in the context of strain gradient elasticity as

$$\begin{Bmatrix} \sigma_x \\ \sigma_y \\ \sigma_{xy} \end{Bmatrix} = (1-l^2\nabla^2) \begin{pmatrix} Q_{11} & Q_{12} & 0 \\ Q_{12} & Q_{22} & 0 \\ 0 & 0 & Q_{66} \end{pmatrix} \begin{Bmatrix} e_x \\ e_y \\ e_{xy} \end{Bmatrix} \tag{11}$$

in which Q_{ij} may be introduced as

$$\begin{aligned} Q_{11} = Q_{22} &= \frac{\tilde{E}}{1-\tilde{\nu}^2}, \\ Q_{12} &= \frac{\tilde{\nu}\tilde{E}}{1-\tilde{\nu}^2},\ Q_{66} = \frac{\tilde{E}}{2(1+\tilde{\nu})} \end{aligned} \tag{12}$$

Here l is called strain gradient coefficient. From integration of Eq. (11) over panel thickness, it may be possible to express the below relations of forces and moments

$$\begin{aligned} N_x &= (1-l^2\nabla^2)[A_{11}e_x^0 + A_{12}e_y^0 \\ &-B_{11}k_x - B_{21}k_y] \end{aligned} \tag{13}$$

$$\begin{aligned} N_y &= (1-l^2\nabla^2)[A_{12}e_x^0 + A_{22}e_y^0 \\ &-B_{12}k_x - B_{22}k_y] \end{aligned} \tag{14}$$

$$N_{xy} = (1-l^2\nabla^2)[+A_{66}e_{xy}^0 - 2B_{66}k_{xy}] \tag{15}$$

$$\begin{aligned} M_x &= (1-l^2\nabla^2)[B_{11}e_x^0 + B_{12}e_y^0 \\ &-D_{11}k_x + D_{12}k_y] \end{aligned} \tag{16}$$

$$\begin{aligned} M_y &= (1-l^2\nabla^2)[B_{12}e_x^0 + B_{22}e_y^0 \\ &-D_{12}k_x - D_{22}k_y] \end{aligned} \tag{17}$$

$$M_{xy} = (1-l^2\nabla^2)[+B_{66}e_{xy}^0 - 2D_{66}k_{xy}] \tag{18}$$

in which ∇^2 is Laplacian operator in Cartesian coordinates and

$$\begin{aligned} A_j &= \int_{-h/2}^{h/2} Q_j dz, \\ B_j &= \int_{-h/2}^{h/2} Q_j z dz, \\ D_j &= \int_{-h/2}^{h/2} Q_j z^2 dz, \\ j &= \{11,12,22,66\} \end{aligned} \tag{19}$$

A curved panel with curvature (R) owns three governing equations which may be calculated employing Hamilton's rule

$$\frac{\partial N_x}{\partial x}+\frac{\partial N_{xy}}{\partial y}=0 \tag{20}$$

$$\frac{\partial N_{xy}}{\partial x}+\frac{\partial N_y}{\partial y}=0 \tag{21}$$

$$\begin{aligned}&\frac{\partial^2 M_x}{\partial x^2}+2\frac{\partial^2 M_{xy}}{\partial x\partial y}+\frac{\partial^2 M_y}{\partial y^2}+\frac{N_y}{R}\\&+N_x(\frac{\partial^2 w}{\partial x^2}+\frac{\partial^2 w^*}{\partial x^2})+2N_{xy}(\frac{\partial^2 w}{\partial x\partial y}+\frac{\partial^2 w^*}{\partial x\partial y})\\&+N_y(\frac{\partial^2 w}{\partial y^2}+\frac{\partial^2 w^*}{\partial y^2})\\&+P_x(\frac{\partial^2 w}{\partial x^2}+\frac{\partial^2 w^*}{\partial x^2})=0\end{aligned} \tag{22}$$

Note that P_x is applied mechanical load in axial direction. Based on the information that A_j, B_j and D_j are functions of x, the governing equations can be re-written by inserting Eqs. (13)-(18) in Eqs. (20) and (22) as

$$\begin{aligned}&(1-l^2\nabla^2)[\frac{\partial}{\partial x}\{A_{11}e_x^0+A_{12}e_y^0\\&-B_{11}k_x-B_{21}k_y\}]\\&+(1-l^2\nabla^2)[\frac{\partial}{\partial y}\{+A_{66}e_{xy}^0-2B_{66}k_{xy}\}]=0\end{aligned} \tag{23}$$

$$\begin{aligned}&(1-l^2\nabla^2)[\frac{\partial}{\partial x}\{+A_{66}e_{xy}^0-2B_{66}k_{xy}\}]\\&+(1-l^2\nabla^2)[\frac{\partial}{\partial y}\{A_{12}e_x^0+A_{22}e_y^0\\&-B_{12}k_x-B_{22}k_y\}]=0\end{aligned} \tag{24}$$

$$\begin{aligned}&(1-l^2\nabla^2)[\frac{\partial^2}{\partial x^2}\{B_{11}e_x^0+B_{12}e_y^0\\&-D_{11}k_x+D_{12}k_y\}]\\&+2(1-l^2\nabla^2)[\frac{\partial^2}{\partial x\partial y}\{+B_{26}e_y^0+B_{66}e_{xy}^0\\&-2D_{66}k_{xy}\}]+(1-l^2\nabla^2)[\frac{\partial^2}{\partial y^2}\{B_{12}e_x^0\\&+B_{22}e_y^0-D_{12}k_x-D_{22}k_y\}]\\&+\frac{1}{R}(1-l^2\nabla^2)[\{A_{12}e_x^0+A_{22}e_y^0\\&-B_{12}k_x-B_{22}k_y\}]+(1-l^2\nabla^2)[\{A_{11}e_x^0\\&+A_{12}e_y^0-B_{11}k_x-B_{21}k_y\}]\frac{\partial^2 w}{\partial x^2}\\&+2(1-l^2\nabla^2)[\{+A_{66}e_{xy}^0-2B_{66}k_{xy}\}]\frac{\partial^2 w}{\partial x\partial y}\\&+(1-l^2\nabla^2)[\{A_{12}e_x^0+A_{22}e_y^0-B_{12}k_x\\&-B_{22}k_y\}]\frac{\partial^2 w}{\partial y^2}+P_x\frac{\partial^2 w}{\partial x^2}=0\end{aligned} \tag{25}$$

4. Solution procedure

In order to solve Eqs. (23)-(25), it is crucial to express the displacements in reliable forms to satisfy the boundary conditions which in the case of simply-support edges become (Barati 2018):

At x=0, L

$$\begin{aligned}&v=w=0,\\&\frac{\partial^2 w}{\partial x^2}=\frac{\partial^2 w}{\partial y^2}=\frac{\partial^4 w}{\partial x^4}=\frac{\partial^4 w}{\partial y^4}=0\end{aligned} \tag{26}$$

At y=0, b

$$\begin{aligned}&u=w=0,\\&\frac{\partial^2 w}{\partial x^2}=\frac{\partial^2 w}{\partial y^2}=\frac{\partial^4 w}{\partial x^4}=\frac{\partial^4 w}{\partial y^4}=0\end{aligned} \tag{27}$$

Then, according to above definitions one can use below approximations for displacement components based on their amplitudes (U , V , W) as

$$u=\sum_{m=1}^{\infty}\sum_{n=1}^{\infty}U_{mn}\frac{\partial f_m^x(x)}{\partial x}f_n^y(y) \tag{28}$$

$$v=\sum_{m=1}^{\infty}\sum_{n=1}^{\infty}V_{mn}f_m^x(x)\frac{\partial f_n^y}{\partial y} \tag{29}$$

$$w=\sum_{m=1}^{\infty}\sum_{n=1}^{\infty}W_{mn}f_m^x(x)f_n^y(y) \tag{30}$$

where the functions $f_m^x=\sin[m\pi x/L]$ and $f_n^y=\sin[n\pi y/b]$ are the applicable functions for satisfying the afore-mentioned conditions. Considering each governing equation as R_i (u, v, w)=0 with (i=1,2,3) and inserting displacement assumptions presented as Eqs. (28)-(30) into R_i yields below equations based upon Galerkin's technique

$$\int_0^b\int_0^L R_1\frac{\partial f_m^x(x)}{\partial x}f_n^y(y)dxdy=0 \tag{31}$$

$$\int_0^b\int_0^L R_2 f_m^x(x)\frac{\partial f_n^y(y)}{\partial y}dxdy=0 \tag{32}$$

$$\int_0^b\int_0^L R_3 f_m^x(x)f_n^y(y)dxdy=0 \tag{33}$$

The weighted residual methods such as Galerkin's method is well discussed in the works of Farrahi *et al.* (2009) and Faghidian *et al.* (2012). By substituting Eqs. (28)-(30) into Eqs. (23)-(25), and using the Galerkin's method, one obtains

$$S_{11}U+S_{21}V+S_{31}W+H_1W^2+Y_1WW^*=0 \tag{34}$$

$$S_{12}U + S_{22}V + S_{32}W + H_2W^2 + Y_2WW^* = 0 \tag{35}$$

$$\begin{aligned} &S_{13}U + S_{23}V + S_{33}W + H_3W^2 + H_4W^3 \\ &+H_5UW + H_6VW + Y_3WW^* \\ &+Y_4W^2W^* + Y_5W\left(W^*\right)^2 + Y_6UW^* \\ &+Y_7VW^* = 0 \end{aligned} \tag{36}$$

in which S_{ij} are linear stiffness matrix components; H_i denotes nonlinear stiffness components and Y_i are added stiffness due to geometric imperfection. With the aid of Eqs. (34) and (35) one can express that

$$\begin{aligned} U &= \frac{S_{21}S_{32} - S_{22}(S_{31} + Y_1W^*)}{S_{11}S_{22} - S_{12}S_{21}}W \\ &+ \frac{H_2S_{21} - H_1S_{22}}{S_{11}S_{22} - S_{12}S_{21}}W^2 \\ V &= \frac{S_{12}S_{31} - S_{11}(S_{32} + Y_2W^*)}{S_{11}S_{22} - S_{12}S_{21}}W \\ &+ \frac{H_1S_{12} - H_2S_{11}}{S_{11}S_{22} - S_{12}S_{21}}W^2 \end{aligned} \tag{37}$$

Then, applying Eq. (37) in Eq. (36) yields a single equation based on W and W^* only. The solution of obtained for finding P_x (GPa) will give post-buckling curves.

5. Results and discussions

Provided in the present section is post-buckling behavior of tapered curved micro-panels reinforced by graphene oxide powders (GOPs) containing epoxy as matrix and GOPs as inclusions. Material properties of the constituents are presented in Table 1. Geometric imperfectness of the micro-panel is also included. The elastic properties of GOP-reinforced materials were determined in the context of Halpin-Tsai scheme incorporating weight fraction of GOPs. The dependency of post-buckling loads on the GOP weight fraction (W_{GOP}), thickness confidents (g_1, g_2), imperfectness (W^*), normalized strain gradient coefficient ($\lambda=l/L$), and curvature radius will be evaluated in detail.

Table 1 Material properties of the constituents

	GOPs	Matrix
Young's modulus (GPa)	E_{GOP}=444.8	E_m=3
Density (kg/m^3)	ρ_{GOP}=1090	ρ_m=1200
Poisson ratio	ν_{GOP}=0.165	ν_m=0.34
Diameter (nm)	d_{GOP}=500	-
Thickness (nm)	t_{GOP}=0.95	-

Table 2 Comparison of post-buckling loads of perfect and imperfect panels for different normalized deflections

$\tilde{W}$	$W^*/h=0$		$W^*/h=0.1$	
	Chikh *et al.* (2016)	present	Chikh *et al.* (2016)	present
0	0.62411	0.62411	0	0
0.1	0.62627	0.62627	0.31853	0.31853
0.2	0.63274	0.63274	0.43334	0.43334
0.3	0.64354	0.64354	0.50047	0.50047

As the first step, post-buckling loads of perfect and imperfect panels are validated in Table 2 with those reported by Chikh *et al.* (2016) considering the gradation of material properties. According to this table, buckling loads have been calculated for both perfect ($W^*/h=0$) and imperfect ($W^*/h=0.1$) panel taking into account various normalized deflection ($\tilde{W}=W/h$). Also, validation of the buckling load of a size-dependent micro-panel with the work of Zhang *et al.* (2015) is presented in Table 3 based on different strain gradient coefficients (l/h=0.1, 0.2, 0.5, 1). Obtained buckling loads are in good agreement with those obtained by Zhang *et al.* (2015).

Depicted in Fig. 2 is the variation of buckling load of micro-size curved panel versus normalized deflection ($\tilde{W}=W/h$) by taking into account different values for geometric imperfection amplitude ($W^*/h=0,$ 0.02, 0.04, 0.06). Strain gradient coefficient is fixed at λ=0.2. It must be clarified that $\tilde{W}=0$ yields a bifurcation point called critical buckling load in the case of perfect micro-panel. However, there is no bifurcation point for an imperfect micro-panel. Therefore, for an imperfect micro-panel the post-buckling load starts from zero and reaches to post-buckling path of the perfect micro-panel at higher values of normalized deflection. Since micro-panels are not always ideal and they may have initial configuration, it is crucial to incorporate their imperfectness effects.

Fig. 3 illustrates buckling load variation versus normalized deflection ($\tilde{W}$) of micro-scale curved panel for various strain gradient coefficient (λ). The panel thickness is considered as constant, therefore the thickness coefficients become $g_1=g_2=0$. For perfect panel it must be stated that $W^*/h=0$ and also for imperfect panel it is assumed that $W^*h=0.02$. The magnitude of GOPs weight fraction is selected as W_{GOP}=0.2% based on uniform GOP distribution. It is found from the figure that higher values for strain gradient coefficient are corresponding to higher post-buckling curves. This is due to additional stiffness of the micro-panel when train gradient effects are included.

Nonlinear buckling load variation of GOP-reinforced curved micro-panels with respect to normalized deflection according to different GOP weight fraction (W_{GOP}) has been plotted in Fig.4. It is assumed that the micro-panel has a curvature radius of R=5L. The present figure indicates that enlarging the magnitude of GOP weight fraction yields greater post-buckling loads. The reason is additional

Table 3 Comparison of non-dimensional buckling load ($\tilde{N} = P_x L^2 / Eh^3$) of micro-panel for different strain g radient coefficients

l/h	Zhang *et al.* (2015)	present
0.1	297.304	297.306
0.2	88.3325	88.3328
0.5	29.7615	29.7617
1	21.3765	21.3768

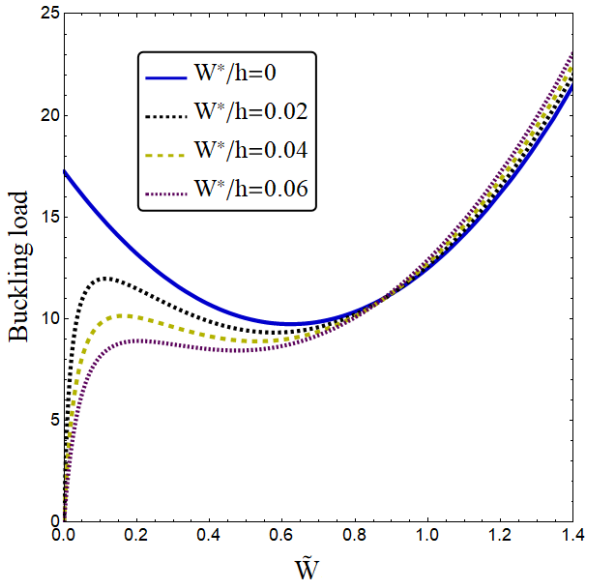

Fig. 2 Buckling load variation versus normalized deflection of cylindrical panel for various magnitude of imperfection (R=5L, h=0.02L, W_{GOP}=0.2%, λ=0.2)

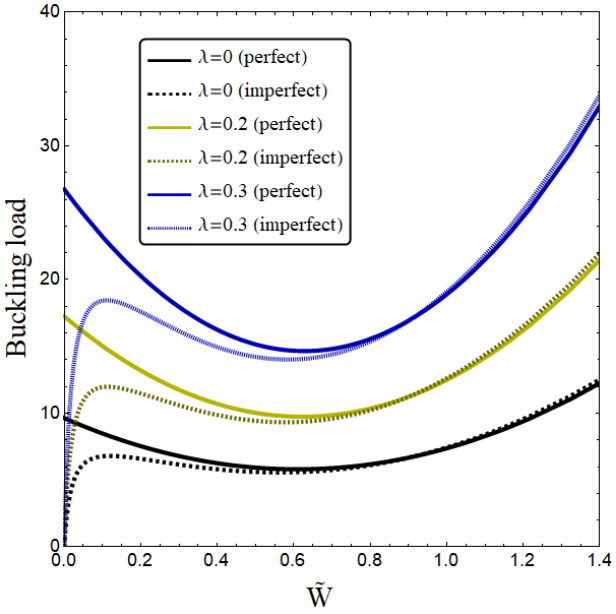

Fig. 3 Buckling load variation versus normalized deflection of cylindrical panel for various strain gradient coefficients (R=5L, h=0.02L, W_{GOP}=0.2%, W*/h=0.02)

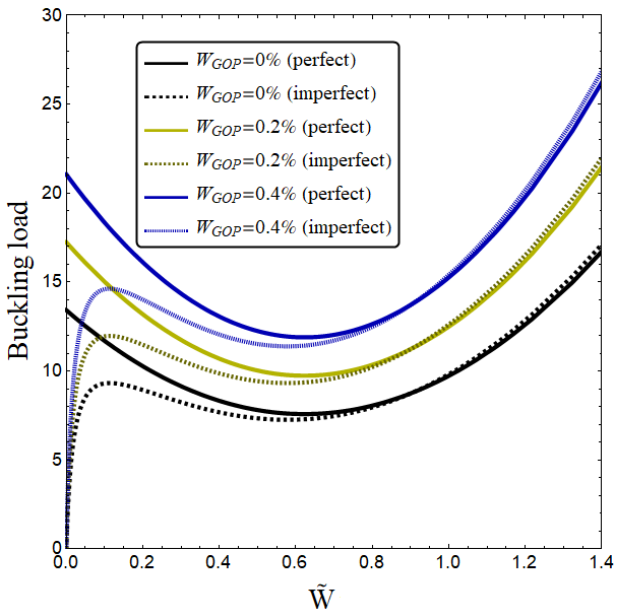

Fig. 4 Buckling load variation versus normalized deflection of cylindrical panel for various GOP weight fractions (R=5L, h=0.02L, λ=0.2, W*/h=0.02)

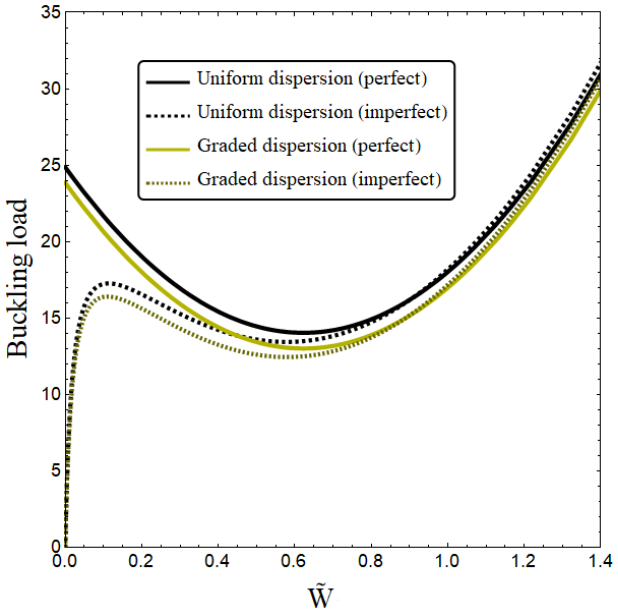

Fig. 5 Buckling load variation versus normalized deflection of cylindrical panel for various GOP dispersion types (R=5L, h=0.02L, W_{GOP}=0.6%, λ=0.2, W*/h=0.02)

stiffness of the micro-scale panel via increase of GOP content. Thus, post-buckling behavior of curved micro-panel may be enhanced via increasing the amount of GOPs in matrix material.

Fig. 5 compares the post-buckling path of the GOP-reinforced micro-panel between uniform and linear distributions of GOPs at a fixed vale of GOP weight fraction W_{GOP}=0.6%. For an imperfect micro-panel it is assumed that W^*/h=0.02. This graph indicates that linear GOP dispersion is corresponding to lower post-buckling load values than uniform GOP dispersion. This is owing to the reason that GOP content is decaying in thickness direction of the micro-panel by considering linear GOP distribution. So, micro-panel based on uniform GOP distribution has extra stiffness compared to linearly graded GOP distribution.

Fig. 6 illustrates the effects of curvature radius (R) on post-buckling curves of GOP-reinforced curved micro-size panel when W_{GOP}=0.2% and λ=0.2. It must be noted that post-buckling curve of flat panels will be derived by

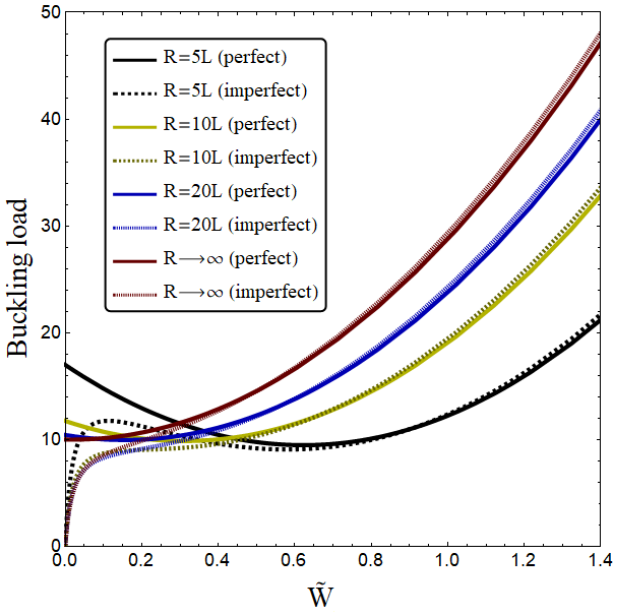

Fig. 6 Buckling load variation versus normalized deflection of cylindrical panel for various curvature radii (h=0.02L, W_{GOP}=0.2%, λ=0.2, W*/h=0.02)

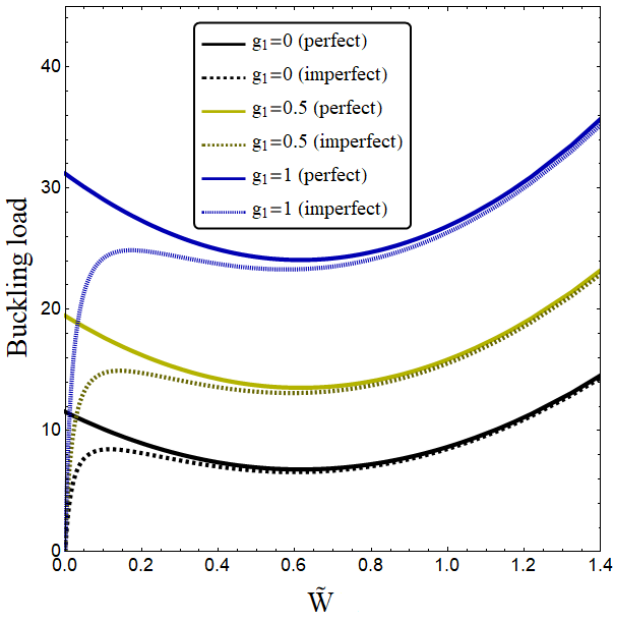

Fig. 7 Buckling load variation versus normalized deflection of cylindrical panel for various first thickness variation parameter (R=5L, h=0.02L, W_{GOP}=0.2%, λ=0.1, g_2=1)

considering curvature radius as infinity (R⟶∞). Indeed, curvature radius specifies the structural behaviors of curved panel. As instance, by increment of curvature radius, the buckling behaviors of curved micro-panels become closer to flat panels. Thus, based on the graph, it can be seen that at smaller values for *R*, buckling loads of perfect micro-panels first decrease with the enlargement of normalized deflection because of remarkable effects of panel curvature. However, at larger values of *R*, buckling load decrement becomes less appreciable.

Variation of post-buckling curves of GOP-reinforced micro-panels based on different values of thickness variation coefficients (g_1, g_2) has been plotted in Figs. 7 and 8 considering perfect and imperfect micro-panel assumptions. By selecting g_2=0 the thickness becomes unvaried; while g_2=1 results in linear thickness changes and g_2=2 results in parabolic thickness changes. Moreover, g_1 denotes a coefficients which evaluates the rates of variation in thickness. One can see that as the magnitude of g_1 is greater, the post-buckling loads are larger. It must be stated

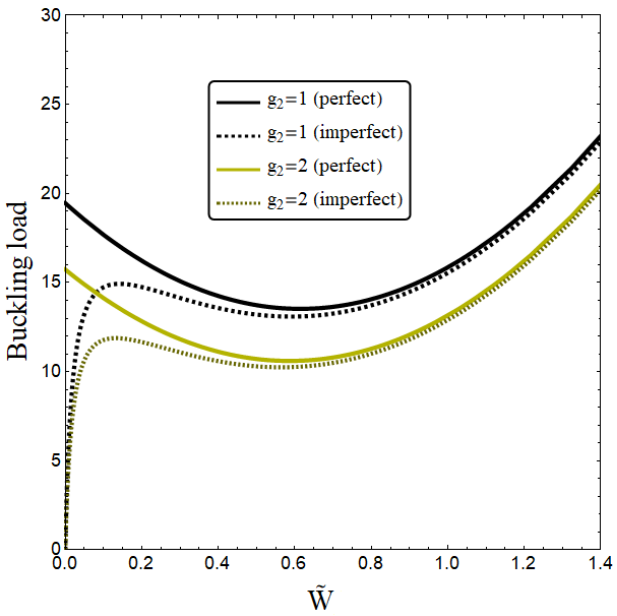

Fig. 8 Buckling load variation versus normalized deflection of cylindrical panel for various second thickness variation parameter (R=5L, h=0.02L, W_{GOP}=0.2%, λ=0.1, g_1=0.5)

that higher values for g_1 results in higher rate of thickness variation. Furthermore, it is obvious that higher values of non-uniform thickness coefficient g_2 results in smaller post-buckling loads.

6. Conclusions

The presented research investigated post-buckling behaviors of geometrically imperfect tapered curved micro-panels made of graphene oxide powder (GOP) reinforced composite. Micro-scale effects on the panel structure were included based on strain gradient elasticity. Post-buckling curves were determined based on both perfect and imperfect micro-panel assumptions. There are some interesting findings which can be classified as:

- For an imperfect micro-panel the post-buckling load starts from zero and reaches to post-buckling path of the perfect micro-panel at higher values of normalized deflection.
- Higher values for strain gradient coefficient are corresponding to higher post-buckling curves.
- Enlarging the magnitude of GOPs weight fraction yields greater post-buckling loads.
- Linear GOP dispersion is corresponding to lower post-buckling load values than uniform GOP dispersion.
- At smaller values for micro-panel curvature, buckling loads of perfect micro-panels first decrease with the enlargement of normalized deflection.
- Higher values of non-uniform thickness coefficient results in smaller post-buckling loads.

Acknowledgements

The first and second authors would like to thank FPQ (Fidar project Qaem) for providing the fruitful and useful help.

References

Abdelaziz, H.H., Meziane, M.A.A., Bousahla, A.A., Tounsi, A., Mahmoud, S.R. and Alwabli, A.S. (2017), "An efficient hyperbolic shear deformation theory for bending, buckling and free vibration of FGM sandwich plates with various boundary conditions", *Steel Compos. Struct.*, **25**(6), 693-704. https://doi.org/10.12989/scs.2017.25.6.693.

Abdulrazzaq, M.A., Fenjan, R.M., Ahmed, R.A. and Faleh, N.M. (2020), "Thermal buckling of nonlocal clamped exponentially graded plate according to a secant function based refined theory", *Steel Compos. Struct.*, **35**(1), 147-157. https://doi.org/10.12989/scs.2020.35.1.147.

Abdulrazzaq, M.A., Kadhim, Z.D., Faleh, N.M. and Moustafa, N. M. (2020), "A numerical method for dynamic characteristics of nonlocal porous metal-ceramic plates under periodic dynamic loads", *Struct. Monit. Maint.*, **7**(1), 27-42. https://doi.org/10.12989/smm.2020.7.1.027.

Abualnour, M., Chikh, A., Hebali, H., Kaci, A., Tounsi, A., Bousahla, A.A. and Tounsi, A. (2019), "Thermomechanical analysis of antisymmetric laminated reinforced composite plates using a new four variable trigonometric refined plate theory", *Comput. Concrete*, **24**(6), 489-498. https://doi.org/10.12989/cac.2019.24.6.489.

Addou, F.Y., Meradjah, M., Bousahla, A.A., Benachour, A., Bourada, F., Tounsi, A. and Mahmoud, S.R. (2019), "Influences of porosity on dynamic response of FG plates resting on Winkler/Pasternak/Kerr foundation using quasi 3D HSDT", *Comput. Concrete*, **24**(4), 347-367. https://doi.org/10.12989/cac.2019.24.4.347.

Ahmed, R.A., Fenjan, R.M. and Faleh, N.M. (2019), "Analyzing post-buckling behavior of continuously graded FG nanobeams

with geometrical imperfections", *Geomech. Eng.*, **17**(2), 175-180. https://doi.org/10.12989/gae.2019.17.2.175.

Ahmed, R.A., Fenjan, R.M., Hamad, L.B. and Faleh, N.M. (2020), "A review of effects of partial dynamic loading on dynamic response of nonlocal functionally graded material beams", *Adv. Mater. Res.*, **9**(1), 33-48. https://doi.org/10.12989/amr.2020.9.1.033.

Ahmed, R.A., Al-Maliki, A.F. and Faleh, N.M. (2020), "Dynamic characteristics of multi-phase crystalline porous shells with using strain gradient elasticity", *Adv. Nano Res.*, **8**(2), 157-167. https://doi.org/10.12989/anr.2020.8.2.157.

Alasadi, A.A., Ahmed, R.A. and Faleh, N.M. (2019), "Analyzing nonlinear vibrations of metal foam nanobeams with symmetric and non-symmetric porosities", *Adv. Aircraft Spacecraft Sci.*, **6**(4), 273-282. https://doi.org/10.12989/aas.2019.6.4.273.

Al-Maliki, A.F., Faleh, N.M. and Alasadi, A.A. (2019), "Finite element formulation and vibration of nonlocal refined metal foam beams with symmetric and non-symmetric porosities", *Struct. Monit. Maint.e*, **6**(2), 147-159. https://doi.org/10.12989/smm.2019.6.2.147.

Al-Maliki, A.F., Ahmed, R.A., Moustafa, N.M. and Faleh, N.M. (2020), "Finite element based modeling and thermal dynamic analysis of functionally graded graphene reinforced beams", *Adv. Comput. Design*, **5**(2), 177-193. https://doi.org/10.12989/acd.2020.5.2.177.

Ali Faghidian, S. (2017), Unified formulations of the shear coefficients in Timoshenko beam theory", *J. Eng. Mech.*, **143**(9), 06017013.

Azimi, M., Mirjavadi, S.S., Shafiei, N. and Hamouda, A.M.S. (2017), "Thermo-mechanical vibration of rotating axially functionally graded nonlocal Timoshenko beam", *Appl. Phys.A*, **123**(1), 104. https://doi.org/10.1007/s00339-016-0712-5.

Bakhadda, B., Bouiadjra, M.B., Bourada, F., Bousahla, A.A., Tounsi, A. and Mahmoud, S.R. (2018), "Dynamic and bending analysis of carbon nanotube-reinforced composite plates with elastic foundation", *Wind Struct.*, **27**(5), 311-324. https://doi.org/10.12989/was.2018.27.5.311.

Barati, M.R. and Zenkour, A.M. (2017), "Post-buckling analysis of refined shear deformable graphene platelet reinforced beams with porosities and geometrical imperfection", *Compos. Struct.*, **181**, 194-202. https://doi.org/10.1016/j.compstruct.2017.08.082.

Barati, M.R. (2018), "A general nonlocal stress-strain gradient theory for forced vibration analysis of heterogeneous porous nanoplates", *Eur. J. Mech.-A/Solids*, **67**, 215-230. https://doi.org/10.1016/j.euromechsol.2017.09.001.

Balubaid, M., Tounsi, A., Dakhel, B. and Mahmoud, S.R. (2019), "Free vibration investigation of FG nanoscale plate using nonlocal two variables integral refined plate theory", *Comput. Concrete*, **24**(6), 579-586. https://doi.org/10.12989/cac.2019.24.6.579.

Batou, B., Nebab, M., Bennai, R., Atmane, H.A., Tounsi, A. and Bouremana, M. (2019), "Wave dispersion properties in imperfect sigmoid plates using various HSDTs", *Steel Compos. Struct.*, **33**(5), 699. https://doi.org/10.12989/scs.2019.33.5.699.

Barretta, R., Faghidian, S.A., Luciano, R., Medaglia, C.M. and Penna, R. (2018), "Free vibrations of FG elastic Timoshenko nano-beams by strain gradient and stress-driven nonlocal models", *Compos. Part B: Eng.*, **154**, 20-32. https://doi.org/10.1016/j.compositesb.2018.07.036.

Belbachir, N., Draich, K., Bousahla, A.A., Bourada, M., Tounsi, A. and Mohammadimehr, M. (2019), "Bending analysis of anti-symmetric cross-ply laminated plates under nonlinear thermal and mechanical loadings", *Steel Compos. Struct.*, **33**(1), 81-92. https://doi.org/10.12989/scs.2019.33.1.081.

Bellal, M., Hebali, H., Heireche, H., Bousahla, A.A., Tounsi, A., Bourada, F. and Tounsi, A. (2020), "Buckling behavior of a single-layered graphene sheet resting on viscoelastic medium via nonlocal four-unknown integral model", *Steel Compos. Struct.*, **34**(5), 643-655. https://doi.org/10.12989/scs.2020.34.5.643.

Boukhlif, Z., Bouremana, M., Bourada, F., Bousahla, A.A., Bourada, M., Tounsi, A. and Al-Osta, M.A. (2019), "A simple quasi-3D HSDT for the dynamics analysis of FG thick plate on elastic foundation", *Steel Compos. Struct.*, **31**(5), 503-516. https://doi.org/10.12989/scs.2019.31.5.503.

Boulefrakh, L., Hebali, H., Chikh, A., Bousahla, A.A., Tounsi, A. and Mahmoud, S.R. (2019), "The effect of parameters of visco-Pasternak foundation on the bending and vibration properties of a thick FG plate", *Geomech. Eng.*, **18**(2), 161-178. https://doi.org/10.12989/gae.2019.18.2.161.

Boutaleb, S., Benrahou, K.H., Bakora, A., Algarni, A., Bousahla, A.A., Tounsi, A. and Mahmoud, S.R. (2019), "Dynamic analysis of nanosize FG rectangular plates based on simple nonlocal quasi 3D HSDT", *Adv. Nano Res.*, **7**(3), 191. https://doi.org/10.12989/anr.2019.7.3.191.

Chikh, A., Bakora, A., Heireche, H., Houari, M.S.A., Tounsi, A. and Bedia, E. . (2016), "Thermo-mechanical postbuckling of symmetric S-FGM plates resting on Pasternak elastic foundations using hyperbolic shear deformation theory", *Struct. Eng. Mech.*, **57**(4), 617-639. https://doi.org/10.12989/sem.2016.57.4.617.

Ebrahimi, F. and Dabbagh, A. (2019), "Vibration analysis of multi-scale hybrid nanocomposite plates based on a Halpin-Tsai homogenization model", *Compos. Part B: Eng.*, **173**, 106955. https://doi.org/10.1016/j.compositesb.2019.106955.

Ebrahimi, F., Nouraei, M. and Dabbagh, A. (2019), "Thermal vibration analysis of embedded graphene oxide powder-reinforced nanocomposite plates", *Eng. with Comput.*, 1-17. https://doi.org/10.1007/s00366-019-00737-w.

Faghidian, S.A., Goudar, D., Farrahi, G.H. and Smith, D.J. (2012), "Measurement, analysis and reconstruction of residual stresses", *J. Strain Anal. Eng.Design*, **47**(4), 254-264.

Faghidian, S.A. (2016), "Unified formulation of the stress field of saint-Venant's flexure problem for symmetric cross-sections", *Int. J. Mech. Sci.*, **111**, 65-72.

Faleh, N.M., Fenjan, R.M. and Ahmed, R.A. (2018), "Dynamic analysis of graded small-scale shells with porosity distributions under transverse dynamic loads", *Eur. Phys. J. Plus*, **133**(9), 348. https://doi.org/10.1140/epjp/i2018-12152-5.

Faleh, N.M., Fenjan, R.M. and Ahmed, R.A. (2020), "Forced vibrations of multi-phase crystalline porous shells based on strain gradient elasticity and pulse load effects", *J. Vib. Eng. Technol.*, 1-9. https://doi.org/10.1007/s42417-020-00203-8.

Fenjan, R.M., Ahmed, R.A., Alasadi, A.A. and Faleh, N.M. (2019), "Nonlocal strain gradient thermal vibration analysis of double-coupled metal foam plate system with uniform and non-uniform porosities", *Coupled Syst. Mech.*, **8**(3), 247-257. https://doi.org/10.12989/csm.2019.8.3.247.

Fenjan, R.M., Ahmed, R.A. and Faleh, N.M. (2019), "Investigating dynamic stability of metal foam nanoplates under periodic in-plane loads via a three-unknown plate theory", *Adv. Aircraft Spacecraft Sci.*, **6**(4), 297-314. https://doi.org/10.12989/aas.2019.6.4.297.

Fenjan, R.M., Hamad, L.B. and Faleh, N.M. (2020), "Mechanical-hygro-thermal vibrations of functionally graded porous plates with nonlocal and strain gradient effects", *Adv. Aircraft Spacecraft Sci.*, 7(2), 169-186. https://doi.org/10.12989/aas.2020.7.2.169.

Farrahi, G.H., Faghidian, S.A. and Smith, D.J. (2009), "An inverse approach to determination of residual stresses induced by shot peening in round bars", *Int. J. Mech. Sci.*, **51**(9-10), 726-731.

Feng, Q. and Meng, F. (2017), "Traveling wave solutions for

fractional partial differential equations arising in mathematical physics by an improved fractional Jacobi elliptic equation method", *Math. Method. Appl. Sci.*, **40**(10), 3676-3686. https://doi.org/10.1002/mma.4254.

Hamad, L.B., Khalaf, B.S. and Faleh, N.M. (2019), "Analysis of static and dynamic characteristics of strain gradient shell structures made of porous nano-crystalline materials", *Adv. Mater. Res.*, **8**(3), 179-196. https://doi.org/10.12989/amr.2019.8.3.179.

Houari, T., Bessaim, A., Houari, M.S.A., Benguediab, M. and Tounsi, A. (2018), "Bending analysis of advanced composite plates using a new quasi 3D plate theory", *Steel Compos. Struct.*, **26**(5), 557-572. https://doi.org/10.12989/scs.2018.26.5.557.

Khalaf, B.S., Fenjan, R.M. and Faleh, N.M. (2019), "Analyzing nonlinear mechanical-thermal buckling of imperfect micro-scale beam made of graded graphene reinforced composites", *Adv. Mater. Res.*, **8**(3), 219. https://doi.org/10.12989/amr.2019.8.3.219.

Kunbar, L.A.H., Alkadhimi, B.M., Radhi, H.S. and Faleh, N.M. (2019), "Flexoelectric effects on dynamic response characteristics of nonlocal piezoelectric material beam", *Adv. Mater. Res.*, **8**(4), 259-274. https://doi.org/10.12989/amr.2019.8.4.259.

Li, X., Li, L., Hu, Y., Ding, Z. and Deng, W. (2017), "Bending, buckling and vibration of axially functionally graded beams based on nonlocal strain gradient theory", *Compos. Struct.*, **165**, 250-265. https://doi.org/10.1016/j.compstruct.2017.01.032.

Marami, G., Nazari, S.A., Faghidian, S.A., Vakili-Tahami, F. and Etemadi, S. (2016), "Improving the mechanical behavior of the adhesively bonded joints using RGO additive", *Int. J. Adhesion Adhesives*, **70**, 277-286.

Mirjavadi, S.S., Rabby, S., Shafiei, N., Afshari, B.M. and Kazemi, M. (2017). On size-dependent free vibration and thermal buckling of axially functionally graded nanobeams in thermal environment", *Appl. Phys. A*, **123**(5), 315. https://doi.org/10.1007/s00339-017-0918-1.

Mirjavadi, S.S., Matin, A., Shafiei, N., Rabby, S. and Mohasel Afshari, B. (2017), "Thermal buckling behavior of two-dimensional imperfect functionally graded microscale-tapered porous beam", *J. Therm. Stresses*, **40**(10), 1201-1214. https://doi.org/10.1080/01495739.2017.1332962.

Mirjavadi, S.S., Afshari, B.M., Khezel, M., Shafiei, N., Rabby, S. and Kordnejad, M. (2018), "Nonlinear vibration and buckling of functionally graded porous nanoscaled beams", *J. Brazilian Soc. Mech. Sci. Eng.*, **40**(7), 352. https://doi.org/10.1007/s40430-018-1272-8.

Mirjavadi, S.S., Mohasel Afshari, B., Shafiei, N., Rabby, S. and Kazemi, M. (2018), "Effect of temperature and porosity on the vibration behavior of two-dimensional functionally graded micro-scale Timoshenko beam", *J. Vib. Control*, **24**(18), 4211-4225. https://doi.org/10.1177%2F1077546317721871.

Mirjavadi, S.S., Afshari, B.M., Barati, M.R. and Hamouda, A.M. S. (2018), "Strain gradient based dynamic response analysis of heterogeneous cylindrical microshells with porosities under a moving load", *Mater. Res. Express*, **6**(3), 035029. https://doi.org/10.1088/2053-1591/aaf5a2.

Mirjavadi, S.S., Afshari, B.M., Barati, M.R. and Hamouda, A.M. S. (2019), "Nonlinear free and forced vibrations of graphene nanoplatelet reinforced microbeams with geometrical imperfection", *Microsyst. Technologies*, **25**(8), 3137-3150. https://doi.org/10.1007/s00542-018-4277-4.

Mirjavadi, S.S., Afshari, B.M., Barati, M.R. and Hamouda, A.M.S. (2019), "Transient response of porous inhomogeneous nanobeams due to various impulsive loads based on nonlocal strain gradient elasticity", *Int. J. Mech. Mater. Design*, 1-12. https://doi.org/10.1007/s10999-019-09452-2.

Mirjavadi, S.S., Forsat, M., Nikookar, M., Barati, M.R. and Hamouda, A.M.S. (2019), "Nonlinear forced vibrations of sandwich smart nanobeams with two-phase piezo-magnetic face sheets", *Eur. Phys. J. Plus*, **134**(10), 508. https://doi.org/10.1140/epjp/i2019-12806-8.

Mirjavadi, S.S., Forsat, M., Barati, M.R., Abdella, G.M., Afshari, B.M., Hamouda, A.M.S. .and Rabby, S. (2019), "Dynamic response of metal foam FG porous cylindrical micro-shells due to moving loads with strain gradient size-dependency", *Eur. Phys. J. Plus*, **134**(5), 214. https://doi.org/10.1140/epjp/i2019-12540-3.

Mirjavadi, S.S., Afshari, B.M., Barati, M.R. and Hamouda, A.M.S. (2019), "Transient response of porous FG nanoplates subjected to various pulse loads based on nonlocal stress-strain gradient theory", *Eur. J. Mech.-A/Solids*, **74**, 210-220. https://doi.org/10.1016/j.euromechsol.2018.11.004.

Muhammad, A.K., Hamad, L.B., Fenjan, R.M. and Faleh, N.M. (2019), "Analyzing large-amplitude vibration of nonlocal beams made of different piezo-electric materials in thermal environment", *Adv. Mater, Res,*, **8**(3), 237-257. https://doi.org/10.12989/amr.2019.8.3.237.

Nguyen, D.D., Kim, S.E., Vu, T.A.T. and Vu, A.M. (2020), "Vibration and nonlinear dynamic analysis of variable thickness sandwich laminated composite panel in thermal environment", *J. Sandw. Struct. Mater.*, 1099636219899402. https://doi.org/10.1177%2F1099636219899402.

Semmah, A., Heireche, H., Bousahla, A.A. and Tounsi, A. (2019), "Thermal buckling analysis of SWBNNT on Winkler foundation by non local FSDT", *Adv. Nano Res.*, **7**(2), 89. https://doi.org/10.12989/anr.2019.7.2.089.

Thanh, C.L., Tran, L.V., Vu-Huu, T. and Abdel-Wahab, M. (2019), "The size-dependent thermal bending and buckling analyses of composite laminate microplate based on new modified couple stress theory and isogeometric analysis", *Comput. Method. Appl. Mech. Eng.*, **350**, 337-361. https://doi.org/10.1016/j.cma.2019.02.028.

Thang, P.T., Duc, N.D. and Nguyen-Thoi, T. (2016), "Effects of variable thickness and imperfection on nonlinear buckling of sigmoid-functionally graded cylindrical panels", *Compos. Struct.*, **155**, 99-106. https://doi.org/10.1016/j.compstruct.2016.08.007.

Tlidji, Y., Zidour, M., Draiche, K., Safa, A., Bourada, M., Tounsi, A. and Mahmoud, S.R. (2019), "Vibration analysis of different material distributions of functionally graded microbeam", *Struct. Eng. Mech.*, **69**(6), 637-649. https://doi.org/10.12989/sem.2019.69.6.637.

Vo, T.P., Thai, H.T., Nguyen, T.K., Lanc, D. and Karamanli, A. (2017), "Flexural analysis of laminated composite and sandwich beams using a four-unknown shear and normal deformation theory", *Compos. Struct.*, **176**, 388-397.

Wu, H., Kitipornchai, S. and Yang, J. (2017), "Thermal buckling and postbuckling of functionally graded graphene nanocomposite plates", *Mater. Design*, **132**, 430-441. https://doi.org/10.1016/j.matdes.2017.07.025.

Zarga, D., Tounsi, A., Bousahla, A.A., Bourada, F. and Mahmoud, S.R. (2019), "Thermomechanical bending study for functionally graded sandwich plates using a simple quasi-3D shear deformation theory", *Steel Compos. Struct.*, **32**(3), 389-410. https://doi.org/10.12989/scs.2019.32.3.389.

Zaoui, F.Z., Ouinas, D. and Tounsi, A. (2019), "New 2D and quasi-3D shear deformation theories for free vibration of functionally graded plates on elastic foundations", *Compos. Part B: Eng.*, **159**, 231-247. https://doi.org/10.1016/j.compositesb.2018.09.051.

Zhang, B., He, Y., Liu, D., Shen, L. and Lei, J. (2015), "An efficient size-dependent plate theory for bending, buckling and

free vibration analyses of functionally graded microplates resting on elastic foundation", *Appl. Math. Model.*, **39**(13), 3814-3845.

Zhang, Z., Li, Y., Wu, H., Zhang, H., Wu, H., Jiang, S. and Chai, G. (2020), "Mechanical analysis of functionally graded graphene oxide-reinforced composite beams based on the first-order shear deformation theory", *Mech. Adv. Mater. Struct.*, **27**(1), 3-11. https://doi.org/10.1080/15376494.2018.1444216.

Zhao, Z., Feng, C., Wang, Y. and Yang, J. (2017), "Bending and vibration analysis of functionally graded trapezoidal nanocomposite plates reinforced with graphene nanoplatelets (GPLs)", *Compos. Struct.*, **180**, 799-808. https://doi.org/10.1016/j.compstruct.2017.08.044.

CC